J|A|C|S
COMMUNICATIONS

Selective Synthesis of $TbMn_2O_5$ Nanorods and $TbMnO_3$ Micron Crystals

Jian-Tao Han,[†] Yun-Hui Huang,*[,†,‡] Wei Huang,[†] and John B. Goodenough[‡]
Laboratory of Advanced Materials, Fudan University, Shanghai 200433, China, and Texas Materials Institute, ETC 9.102, The University of Texas at Austin, Austin, Texas 78712

Received July 31, 2006; E-mail: huangyh@mail.utexas.edu

Multiferroic materials, in which more than one of ferromagnetic, ferroelectric, and ferroelastic properties appear simultaneously, have received renewed interest in recent years because of potential applications in new devices based on the mutual controls of magnetic and electric fields.[1] Many efforts have been devoted to finding new multiferroic materials or to investigating multiferroic properties in known oxides, such as $BiCrO_3$,[2] $BiMnO_3$,[3] $BiFeO_3$,[4] $BiCoO_3$,[5] $BiNiO_3$,[6] $BiScO_3$,[7] and double perovskite Bi_2MnNiO_6.[8] Recently, multiferroic effects have been found in some rare earth manganates. Hur et al. reported a profound interplay between electrical polarization and the applied magnetic field in $TbMn_2O_5$.[9] Kimura et al. observed giant magnetocapacitance and magnetoelectric effects in $TbMnO_3$.[10]

For most multiferroic perovskite oxides, a high-pressure technique is required to get a single phase. Not only is the equipment for the synthesis complicated, but also the microstructure of the sample cannot be controlled well. As is well-known, the properties of the samples strongly depend on their morphologies, sizes, and defect densities.[11] Thus the synthesis method is important for the functional materials. Our previous work on $BiFeO_3$ nanospindles showed that a facile, mild, and easily controlled hydrothermal route is available to synthesize multiferroic materials with uniform microstructure.[12] In this Communication, we describe a one-pot selective synthesis of multiferroic $TbMn_2O_5$ nanorods and $TbMnO_3$ micrometer crystals with a convenient hydrothermal route.

All chemicals were purchased from Shanghai Chemical Reagents Company and used without further purification. For a typical synthesis of $TbMn_2O_5$ nanorods, 1.4 mmol $MnCl_2{\cdot}H_2O$, 0.6 mmol $KMnO_4$, 1.0 mmol $Tb(NO_3)_3{\cdot}6H_2O$ and 0.5 mol NaOH were dissolved in distilled water. After stirring for half an hour, the homogeneous solution was transferred into an 80 mL Teflon-lined steel autoclave and heated at 250 °C for 72 h. $TbMnO_3$ micrometer crystals were obtained via the same procedure as $TbMn_2O_5$ nanorods by just changing the molar ratio of reactants $MnCl_2{\cdot}4H_2O$ and $KMnO_4$ from 7:3 to 4:1.

The crystallinity and purity of the products were examined by X-ray diffraction (XRD) measurements on a Bruker X-ray diffractometer with Cu Kα radiation. XRD patterns of freshly prepared $TbMn_2O_5$ nanorods and $TbMnO_3$ crystals are shown in Figure 1. All diffraction peaks of $TbMn_2O_5$ can be perfectly indexed by an orthorhombic phase with space group *Pbam* (No. 55). The lattice parameters, refined with the Rietveld program MAUD,[13] are $a = 7.3272(2)$, $b = 8.5223(1)$, and $c = 5.6776(2)$ Å (Figure S1). For $TbMnO_3$, the peaks can be indexed to an orthorhombically distorted perovskite phase with space group *Pbnm* (No. 62). The lattice constants are: $a = 5.3011(2)$, $b = 5.8510(1)$, and $c = 7.4006(3)$ Å (Figure S2). X-ray photoelectron spectroscopy (XPS, PHI Quantera SXM) shows that both $TbMn_2O_5$ and $TbMnO_3$ consist of Tb, Mn, and O elements. The Mn $2p_{3/2}$ binding energy of 641.8 eV is a characteristic of Mn^{3+} (Figures S4b).[14] The Mn 2p doublet of $TbMn_2O_5$ shifts by 0.7 eV toward higher binding energy compared to the Mn 2p doublet of $TbMnO_3$, which is evident for a mixed $Mn^{4+/3+}$ state in $TbMn_2O_5$.[15]

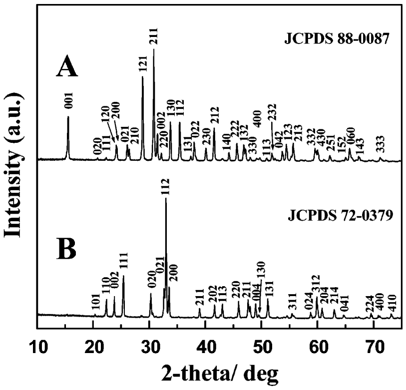

Figure 1. XRD patterns of (A) $TbMn_2O_5$ and (B) $TbMnO_3$.

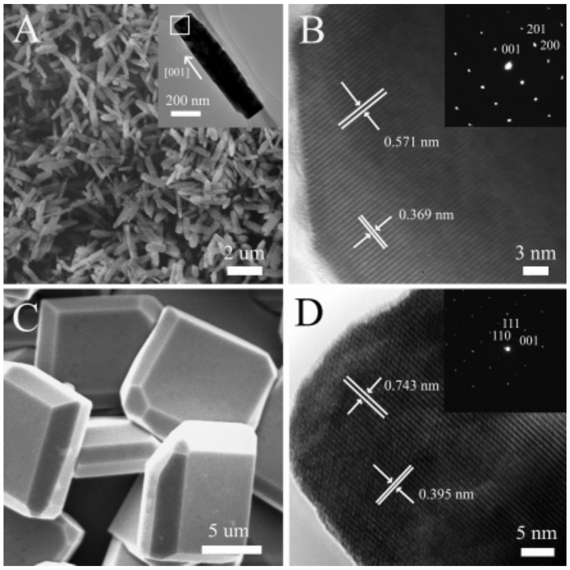

Figure 2. (A) SEM image of $TbMn_2O_5$ nanorods; right inset shows the TEM image of a single $TbMn_2O_5$ nanorod; (B) HRTEM image of the same nanorod; right inset shows a SAED pattern of the same nanorod; (C) SEM image of $TbMnO_3$ crystals; (D) HRTEM image of a single $TbMnO_3$ micron crystal; right inset shows a SAED pattern of the same crystal.

The morphology and microstructure of the samples were investigated with scanning electron microscopy (SEM, SHIMDAZU SSX-550). As shown in Figure 2A, $TbMn_2O_5$ particles exhibit a uniform, rodlike morphology with an average size of about 2 μm in length and 200 nm in diameter. We further examined the microstructure with transmission electron microscopy (TEM) and high-resolution TEM (FEI CM-200 at 160 kV). The inset of Figure 2A shows a low-magnification TEM image of a typical $TbMn_2O_5$ nanorod. The selected area electron diffraction (SAED) pattern in the inset of Figure 2B, taken along the [010] zone axis from an

---

[†] Fudan University.
[‡] The University of Texas at Austin.

10.1021/ja065520u CCC: $33.50 © 2006 American Chemical Society

individual nanorod with very sharp diffraction spots, indicates that the as-prepared $TbMn_2O_5$ nanorods consist of single crystals that grow along the [001] direction (the *c*-axis). Moreover, the SEAD images taken from different positions along the nanorod (without tilting the sample with respect to the electron beam) are found to be almost identical, which demonstrates that the entire nanorod is one perfect single crystal. The corresponding HRTEM image (Figure 2B) shows interplanar distances of 0.571 and 0.369 nm, which correspond to (001) and (200) planes, respectively. Figure 2C shows an SEM image of as-prepared $TbMnO_3$. Its morphology is quite different from that of $TbMn_2O_5$. Micron crystals with flat faces and regular shapes are observed. Figure 2D shows a HRTEM micrograph of a $TbMnO_3$ crystal with clearly resolved interplanar distances $d_{001} = 0.743$ nm and $d_{110} = 0.395$ nm.

To gain further insight into the structural features of $TbMn_2O_5$ nanorods and $TbMnO_3$ crystals, unpolarized Raman-scattering spectra (Jobin-Yvon HR800) were measured with a liquid-nitrogen-cooled CCD camera in the backscattering geometry at 298 K (Figures S3). Ten Raman peaks at 108, 174, 212, 237, 649, 497, 535, 624, 668, and 688 cm^{-1} are observed in $TbMn_2O_5$; whereas five Raman peaks at 376, 487, 505, 526, and 609 cm^{-1} are observed in $TbMnO_3$. The highest-frequency peaks appear at 609 and 588 cm^{-1} for $TbMn_2O_5$ and $TbMnO_3$, respectively; these peak positions are well consistent with reported data.[16]

The $TbMn_2O_5$ structure with space group *Pbam* consists of $Mn^{4+}O_6$ octahedra and $Mn^{3+}O_5$ pyramids. The octahedra share edges to form ribbons parallel to the *c*-axis, and adjacent ribbons are connected by pairs of corner-sharing pyramids. $TbMnO_3$ has an orthorhombic perovskite structure that is quite different from $TbMn_2O_5$. Under the high-pressure condition of a hydrothermal process, the redox reaction between $KMnO_4$ and $MnCl_2$ in an alkaline solution can be carried out completely, and the Mn valence in the product depends on the molar ratio of Mn^{7+} and Mn^{2+} ions in the reactants. Therefore, the molar ratio of Mn^{7+} and Mn^{2+} is critical to the final product. The formation of $TbMn_2O_5$ and $TbMnO_3$ can be written as follows:

$$5Tb(NO_3)_3 + 3KMnO_4 + 7MnCl_2 + 26NaOH \rightarrow 5TbMn_2O_5 + 12NaNO_3 + 14NaCl + 3KNO_3 + 13H_2O \quad (1)$$

$$5Tb(NO_3)_3 + KMnO_4 + 4MnCl_2 + 22NaOH \rightarrow 5TbMnO_3 + 14NaNO_3 + 8NaCl + KNO_3 + 11H_2O \quad (2)$$

In the hydrothermal process, the size and the morphology of the product depend on the competition between crystal nucleation and crystal growth, which are determined by the inherent crystal structure and the chemical potential in the precursor solution. The differences in size and shape between $TbMn_2O_5$ and $TbMnO_3$ are ascribed to their different structures and the speed of the redox reactions.

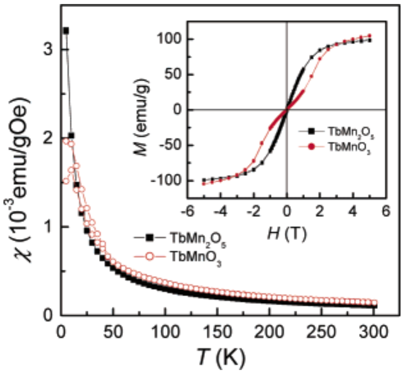

Figure 3. Temperature dependence of zero-field-cooled (ZFC) and field-cooled (FC) susceptibility (χ) measured in a field of 100 Oe for $TbMn_2O_5$ and $TbMnO_3$. The inset shows their field-dependent magnetization at 5 K.

Figure 3 shows magnetic susceptibility $\chi(T)$ and magnetic hysteresis loops for the $TbMn_2O_5$ nanorods and the $TbMnO_3$ micrometer crystals. No difference is observed between the zero-field-cooled (ZFC) and field-cooled (FC) susceptibility curves of $TbMn_2O_5$. Above 50 K, the susceptibility obeys the Curie−Weiss law, $\chi = C/(T - \theta)$, with $\theta = -28$ K; below 50 K, the $\chi(T)$ curve increases dramatically owing to a weak ferromagnetism below a Néel temperature T_N near 50 K. For $TbMnO_3$, a separation between the ZFC and the FC curves is observed below 44 K, and an anomaly occurs around 8 K; 44 and 8 K correspond, respectively, to the T_N due to the Mn^{3+} spins and the ordering temperature of the Tb^{3+} spins.[17] The $M(H)$ of $TbMnO_3$ at 5 K shows a two-step magnetization process, which may be ascribed to the spin reorientation of Tb^{3+} ions in Mn^{3+} sites owing to Tb^{3+} spin reversal.[10] For both samples, a slight magnetic hysteresis is observed at 5 K, and the magnetization is almost saturated at high field, which is due to a weak ferromagnetism of Mn arrays.

Acknowledgment. We thank Prof. Xiao-Jing Wu in Fudan University for TEM measurement and financial support by the National Natural Science Foundation of China (Grant Nos. 60371011, 60235412, 60490290, and 90406021).

Supporting Information Available: The lattice parameters based on the Rietveld refinement of the X-ray powder diffraction data; Raman patterns and XPS spectra of $TbMn_2O_5$ and $TbMnO_3$. This material is available free of charge via the Internet at http://pubs.acs.org.

References

(1) (a) Hill, N. A. *J. Phys. Chem. B* **2000**, *104*, 6694. (b) Wang, J.; Neaton, J. B.; Zheng, H.; Nagarajan, V.; Ogale, S. B.; Liu, B.; Viehland, D.; Vaithyanathan, V.; Schlom, D. G.; Waghmare, U. V.; Spaldin, N. A.; Rabe, K. M.; Wutting, M.; Ramesh, R. *Science* **2003**, *299*, 1719. (c) Lottermoser, T.; Lonkai, T.; Amann, U.; Hohlwein, D.; Ihringer, J.; Fiebig, M. *Nature* **2004**, *430*, 541.
(2) Niitaka, S.; Azuma, M.; Takano, M.; Nishibori, E.; Takata, M.; Sakata, M. *Solid State Ionics* **2004**, *172*, 557.
(3) (a) Montanari, E.; Calestani, G.; Migliori, A.; Dapiaggi, M.; Bolzoni, F.; Cabassi, R.; Gilioli, E. *Chem. Mater.* **2005**, *17*, 6457. (b) Montanari, E.; Righi, L.; Calestani, G.; Migliori, A.; Gilioli, E.; Bolzoni, F. *Chem. Mater.* **2005**, *17*, 1765.
(4) (a) Wang, Y.; Jiang, Q. H.; He, H. C.; Nan, C. W. *Appl. Phys. Lett.* **2006**, *88*, 142503. (b) Baettig, P.; Ederer, C.; Spaldin, N. A. *Phys. Rev. B* **2005**, *72*, 214105.
(5) Belik, A. A.; Iikubo, S.; Kodama, K.; Igawa, N.; Shamoto, S.; Niitaka, S.; Azuma, M.; Shimakawa, Y.; Takano, M.; Izumi, F.; Takayama-Muromachi, E. *Chem. Mater.* **2006**, *18*, 798.
(6) Ishiwata, S.; Azuma, M.; Takano, M.; Nishibori, E.; Takata, M.; Sakata, M.; Kato, K. *J. Mater. Chem.* **2003**, *13*, 432.
(7) Belik, A. A.; Iikubo, S.; Kodama, K.; Igawa, N.; Shamoto, S.; Maie, M.; Nagai, T.; Matsui, Y.; Stefanovich, S. Y.; Lazoryak, B. I.; Takayama-Muromachi, E. *J. Am. Chem. Soc.* **2006**, *128*, 706.
(8) Azuma, M.; Takata, K.; Saito, T.; Ishiwata, S.; Shimakawa, Y.; Takano, M. *J. Am. Chem. Soc.* **2005**, *127*, 8889.
(9) Hur, N.; Park, S.; Sharma, P. A.; Ahn, J. S.; Guha, S.; Cheong, S. W. *Nature* **2004**, *429*, 392.
(10) Kimura, T.; Goto, T.; Shintani, H.; Ishizaka, K.; Arima, T.; Tokura, Y. *Nature* **2003**, *426*, 55.
(11) Feng, S. H.; Xu, R. R. *Acc. Chem. Res.* **2001**, *34*, 239.
(12) Han, J. T.; Huang, Y. H.; Wu, X. J.; Wu, C. L.; Wei, W.; Peng, B.; Huang, W.; Goodenough, J. B. *Adv. Mater.* **2006**, *18*, 2145.
(13) Maud - Materials Analysis Using Diffraction, Version 2.046 (July 21, 2006); http://www.ing.unitn.it/∼maud/.
(14) Kang, J. S.; Han, S. W.; Park, J. G.; Wi, S. C.; Lee, S. S.; Kim, G.; Song, H. J.; Shin, H. J.; Jo, W.; Min, B. I. *Phys. Rev. B* **2005**, *71*, 092405.
(15) Beyreuther, E.; Grafstrom, S.; Eng, L. M.; Thiele, C.; Dorr, K. *Phys. Rev. B* **2006**, *73*, 155425.
(16) (a) Mihailova, B.; Gospodinov, M. M.; Guttler, B.; Yen, F.; Litvinchuk, A. P.; Iliev, M. N. *Phys. Rev. B* **2005**, *71*, 172301. (b) Iliev, M. N.; Abrashev, M. V.; Laverdiere, J.; Jandl, S.; Gospodinov, M. M.; Wang, Y. Q.; Sun, Y. Y. *Phys. Rev. B* **2006**, *73*, 064302.
(17) Huang, Y. H.; Fjellvag, H.; Karppinen, M.; Hauback, B. C.; Yamauchi, H.; Goodenough, J. B. *Chem. Mater.* **2006**, *18*, 2130.

JA065520U